Paper III

Long-Range Persistence in Global Surface Temperatures Explained by Linear Multibox Energy Balance Models

Journal of Climate, **30**, 7157 – 7168, 2017

Long-Range Persistence in Global Surface Temperatures Explained by Linear Multibox Energy Balance Models

Hege-Beate Fredriksen and Martin Rypdal

Department of Mathematics and Statistics, University of Tromsø—The Arctic University of Norway, Tromsø, Norway

(Manuscript received 6 December 2016, in final form 9 April 2017)

ABSTRACT

The temporal fluctuations in global mean surface temperature are an example of a geophysical quantity that can be described using the notions of long-range persistence and scale invariance/scaling, but this description has suffered from lack of a generally accepted physical explanation. Processes with these statistical signatures can arise from nonlinear effects, for instance, through cascade-like energy transfer in turbulent fluids, but they can also be produced by linear models with scale-invariant impulse–response functions. This paper demonstrates that, on time scales from months to centuries, the scale-invariant impulse–response function of global surface temperature can be explained by simple linear multibox energy balance models. This explanation describes both the scale invariance of the internal variability and the lack of a characteristic time scale of the response to external forcings. With parameters estimated from observational data, the climate response is approximately scaling in these models, even if the response function is not chosen to be scaling a priori. It is also demonstrated that the differences in scaling exponents for temperatures over land and for sea surface temperatures can be reproduced by a version of the multibox energy balance model with two distinct surface boxes.

1. Introduction

Instrumental measurements and proxy reconstructions of Earth's surface temperatures show temporal variability on a range of different time scales (Lovejoy 2015; Huybers and Curry 2006). For the global mean surface temperature (GMST), the variability can be parsimoniously described as scale invariant, since the estimated power spectral densities (PSDs) are well approximated by power laws $S(f) \sim 1/f^{\beta}$ from monthly to centennial scales (Rypdal et al. 2013). The typical scaling exponent is $\beta \approx 1$, and the signals are well described as a so-called $1/f$ noise, or pink noise. Some of the low-frequency variability in the temperature records can be accounted for by the variability in the radiative forcing of the planet, but even the residual fluctuations are well described as a scaling stochastic process, with a slightly lower exponent β. This suggests that scale-invariant dynamics is an intrinsic property of the climate system, a claim that is supported by the observation of scaling PSDs in unforced control runs of general circulation models (GCMs), on time scales from months to centuries (Fredriksen and Rypdal 2016; Rybski et al. 2008; Fraedrich and Blender 2003).

A signal with power-law PSD can be modeled as a stochastic process with long-range dependence (LRD), and examples of such processes are the fractional Gaussian noises (fGns) and the fractional autoregressive integrated moving average (FARIMA) models. Stochastic processes that exhibit LRD provide more accurate descriptions of the unforced GMST variability compared to the traditional red noise models, such as the Ornstein–Uhlenbeck (OU) processes and the autoregressive processes of order 1 [AR(1)] (Rypdal and Rypdal 2014). The latter are characterized by a single time scale, and are incapable of describing the multiscale nature of the climate fluctuations. Despite this, the LRD processes are largely ignored by many climate scientists, and some consider LRD to be an exotic and redundant notion in climate science (Mann 2011).

Denotes content that is immediately available upon publication as open access.

Corresponding author: Hege-Beate Fredriksen, hege-beate.fredriksen@uit.no

DOI: 10.1175/JCLI-D-16-0877.1

One of the aims of this paper is therefore to demystify the notion of LRD in the climate system by demonstrating that the observed phenomena can be produced by simple multibox energy balance models (EBMs). With this, we demonstrate that the exotic physics may be no more than vertical heat conduction in the ocean and that it is reasonable to think of LRD as an approximation to the linear response of EBMs with multiple characteristic time scales. Only a few boxes are needed to obtain power-law PSDs on scales from months to centuries. We also demonstrate how we can construct box models that are consistent with the observation that the exponent β is lower for land temperatures than for sea surface temperatures (SSTs) (Fredriksen and Rypdal 2016).

Only a few of the studies that analyze LRD in surface temperatures focus on the mechanisms behind the phenomenon (e.g., Fraedrich 2002; Fraedrich and Blender 2003; Fraedrich et al. 2004; Blender et al. 2006; Franzke et al. 2015). Most treat LRD processes merely as statistical models that fit well with data (Vyushin et al. 2012; Rybski et al. 2006; Franzke 2010). Statistical inference for LRD processes requires special care to avoid the fallacy of circular reasoning: that is, falsely attributing trends in the forced signal to natural variability (Benestad et al. 2016). Incautious trend-significance testing using LRD null models (Cohn and Lins 2005) have led some climate scientists to view LRD processes as exotic mathematical objects that somehow fit with the ‘‘climate denier agenda’’ (Mann 2011; Benestad et al. 2016). This is paradoxical, since climate response models that exhibit LRD actually display more ‘‘heating in the pipeline,’’ and, compared with other response models, they predict that emissions of greenhouse gases must be reduced earlier and more drastically to avoid dangerous anthropogenic influence (K. Rypdal 2016; Rypdal and Rypdal 2014).

Other climate scientists consider scaling to be an inherent property of atmospheric turbulent flows and certain types of regime switching dynamics (Lovejoy and Schertzer 2013; Franzke et al. 2015) and, as such, a signature of the nonlinearity of the underlying dynamics. In fact, Huybers and Curry (2006) hypothesize that the persistent scaling of surface temperatures observed on decadal to multicentennial scales is due to a nonlinear cascade driven by the seasonal forcing. They present a bicoherence spectrum in favor of this hypothesis, but the phase correlations that give rise to high bicoherence do not imply an effective nonlinear energy transfer between the seasonal and the multidecadal scales. We have also had problems in reproducing the bicoherence spectra reported in this paper. In a forthcoming paper, we will examine this hypothesis in depth.

Since the ocean has a large heat capacity compared to the atmosphere, the observation that ocean temperatures are more persistent than land temperatures (Fraedrich and Blender 2003; Fredriksen and Rypdal 2016) is an indication that the observed persistence in global temperature to a larger extent must be attributed to ocean heat content and ocean dynamics and to a lesser extent to nonlinear processes in the atmosphere. This hypothesis is further strengthened by the results of Fraedrich and Blender (2003), who find that only models with full ocean circulation show persistence on scales longer than about a decade. In the present paper, we model the slowly responding components of the climate system by including ‘‘boxes’’ that exchange heat with the more rapidly responding mixed layer. This is clearly an oversimplification of the ocean dynamics but reproduces the multiscale characteristics of the surface temperature response.

The paper is structured as follows. Section 2 discusses the construction of multibox EBMs and their corresponding response functions, and in section 3 we demonstrate how the superposition of different response times can be used to approximate an LRD response. Furthermore, we estimate parameters and explore how the response of sea surface temperatures differs from the response of land temperatures. Section 4 presents some concluding discussions.

2. Multibox EBMs

The simplest climate model we can imagine is the so-called one-box EBM for the global temperature:

$$C\frac{d\Delta T}{dt} = -\frac{1}{S_{\mathrm{eq}}}\Delta T + \Delta F(t). \qquad (1)$$

In this equation, C denotes the average heat capacity per square meter of the surface, ΔT is the temperature anomaly relative to an equilibrium state, S_{eq} is the equilibrium climate sensitivity, and $\Delta F(t)$ is the forcing (i.e., the perturbation of effective radiative forcing from the initial equilibrium state $\Delta T = 0$). As a response to a constant perturbation ΔF, the temperature will reach a new equilibrium ΔT, and the change in equilibrium temperature relative to the change in radiative forcing is equal to the equilibrium climate sensitivity: that is,

$$S_{\mathrm{eq}} = \frac{\Delta T}{\Delta F}.$$

For a time-dependent forcing $\Delta F(t)$, the temperature $\Delta T(t)$ is given by a convolution integral

$$\Delta T(t) = \int_{-\infty}^{t} R(t-s)\Delta F(s)\,ds, \qquad (2)$$

where the impulse–response function is an exponentially decaying function with a characteristic time scale $\tau = CS_{\mathrm{eq}}$:

$$R(t) = \frac{1}{C} e^{-t/\tau}. \tag{3}$$

In the one-box model there is no heat exchange with the deep ocean, but this can be included by extending the model to also include a box with a larger heat capacity C_2. If the energy exchange between the upper and lower box is proportional to the temperature difference between the two boxes, we obtain what is known as the two-box EBM (Geoffroy et al. 2013; Held et al. 2010; Rypdal 2012; Caldeira and Myhrvold 2013):

$$C_1 \frac{d\Delta T_1}{dt} = -\frac{1}{S_{\mathrm{eq}}} \Delta T_1 + \kappa_2(\Delta T_2 - \Delta T_1) + \Delta F(t) \quad \text{and} \tag{4}$$

$$C_2 \frac{d\Delta T_2}{dt} = -\kappa_2(\Delta T_2 - \Delta T_1). \tag{5}$$

The equations can be written in matrix form:

$$\mathbf{C} \frac{d\Delta\mathbf{T}}{dt} = \mathbf{K}\Delta\mathbf{T} + \Delta\mathbf{F}(t), \tag{6}$$

where we introduce the notation

$$\mathbf{C} = \begin{bmatrix} C_1 & 0 \\ 0 & C_2 \end{bmatrix}, \quad \Delta\mathbf{T} = \begin{bmatrix} \Delta T_1 \\ \Delta T_2 \end{bmatrix}, \quad \text{and} \quad \Delta\mathbf{F}(t) = \begin{bmatrix} \Delta F(t) \\ 0 \end{bmatrix}$$

and

$$\mathbf{K} = \begin{bmatrix} -(\kappa_1 + \kappa_2) & \kappa_2 \\ \kappa_2 & -\kappa_2 \end{bmatrix}. \tag{7}$$

For convenience, we denote $\kappa_1 = 1/S_{\mathrm{eq}}$, but it should be noted that the physical meaning of κ_1 is different from κ_2. While κ_2 is a coefficient of heat transfer between two ocean layers, κ_1 is determined by the linearized response of the net outgoing radiation to changes in the surface temperature. It includes all the atmospheric feedbacks and is sometimes referred to as the equilibrium global climate feedback (Armour et al. 2013), or simply the "feedback parameter."

The natural generalization of the two-box model is to consider N vertically distributed boxes. The model is formulated as in Eq. (6), with $\Delta\mathbf{T}$ and $\Delta\mathbf{F}$ being N vectors and $\mathbf{C}$ and $\mathbf{K}$ being $N \times N$ matrices. The matrix $\mathbf{C}$ will be a diagonal matrix with the heat capacities of each box along the diagonal, and $\mathbf{K}$ will be a tridiagonal matrix. The forcing vector $\Delta\mathbf{F}$ consists of zeros for all boxes not connected to the surface. We note that, when N is large, this model setup can approximate a vertical diffusion model.

In an N-box EBM the N-vector temperature can be written using matrix-exponential notation:

$$\Delta\mathbf{T}(t) = \int_{-\infty}^{t} e^{(t-s)\mathbf{A}} \mathbf{C}^{-1} \Delta\mathbf{F}(s)\, ds, \quad \text{with} \quad \mathbf{A} = \mathbf{C}^{-1}\mathbf{K},$$

and it follows that the surface temperature is given by a convolution integral similar to the one in Eq. (2), but where the impulse–response function is now a weighted sum of N exponentially decaying functions:

$$R(t) = (e^{t\mathbf{A}}\mathbf{C}^{-1})_{11} = \sum_{k=1}^{N} b_k e^{-t/\tau_k}. \tag{8}$$

The characteristic time scales are defined as $\tau_k = -1/\lambda_k$ for $k = 1, \ldots, N$, where λ_k are the eigenvalues of the matrix $\mathbf{C}^{-1}\mathbf{K}$. Since $-\mathbf{K}$ is symmetric and positive definite, the eigenvalues λ_k are real and negative.

The model defined by Eq. (6) is meant to describe vertically distributed boxes, but boxes can also be aligned horizontally. This can be useful in order to include the atmosphere over land in the model. In principle, we can have interactions between all boxes, making the matrix $\mathbf{K}$ less sparse. The mathematical form of the response function remains the same though, but the characteristic time scales and the weights b_k are changed. Several horizontally distributed boxes could also be useful for modeling a space-dependent depth of the mixed layer.

To make separate boxes for the upper ocean layer and atmosphere over land, we adopt the asymmetric heat exchange between land and sea used by Meinshausen et al. (2011) to obtain the equations

$$C_L \frac{d\Delta T_L}{dt} = -\lambda_L \Delta T_L + F_L(t) + \frac{k}{f_L}(\mu\alpha\Delta T_1 - \Delta T_L) \quad \text{and}$$
$$C_1 \frac{d\Delta T_1}{dt} = -\lambda_O \Delta T_1 + F_O(t) - \frac{k}{f_O}(\mu\alpha\Delta T_1 - \Delta T_L) + F_N. \tag{9}$$

Here it is assumed that the temperature in the atmosphere over oceans $\Delta T_{O,\mathrm{atmos}}$ is proportional to the temperature in the mixed layer (i.e., $\Delta T_{O,\mathrm{atmos}} = \alpha\Delta T_1$), where the factor $\alpha > 1$ describes the effect of changing sea ice cover (Raper et al. 2001). The parameter $\mu > 1$ quantifies the asymmetry in the heat transport between the atmosphere over the ocean and the atmosphere over land. The parameter $f_L = 0.29$ is the proportion of Earth's surface that is covered by land, and $f_O = 1 - f_L$. The term F_N represents the heat transport into the deep oceans, and F_L and F_O are the forcing terms over land and ocean, respectively. From models in phase 3 of the Coupled Model Intercomparison Project (CMIP3), one finds that the typical values of μ are in the range 1–1.4 (Meinshausen et al. 2011). This implies that, when a new equilibrium is reached after a perturbation of the forcing, the land temperature will have changed more than the SST.

In the limit $C_L \to 0$, Eq. (9) becomes

$$\Delta T_L = \frac{F_L(t) + k\mu\alpha\Delta T_1/f_L}{\lambda_L + k/f_L}. \qquad (10)$$

Hence, land temperature appears as a weighted sum of the SST and an instantaneous response to the forcing over land. The GMST anomaly is given by

$$\Delta T_{\text{global}} = f_L\Delta T_L + f_O\Delta T_1 = \left(f_O + \frac{k\mu\alpha}{\lambda_L + k/f_L}\right)\Delta T_1 + \frac{f_L}{\lambda_L + k/f_L}F_L(t).$$

3. Approximate scale invariance from aggregation of OU processes

The Ornstein–Uhlenbeck stochastic process is defined via the stochastic differential equation

$$dx(t) = -\theta x(t)\,dt + \sigma dB(t),$$

where $dB(t)$ is the measure of white noise. The equation has a stationary solution of the form

$$x(t) = \int_{-\infty}^{t} R(t-s)\,dB(s), \quad \text{with} \quad R(t) = \sigma e^{-\theta t}. \qquad (11)$$

The parameter σ is called the scale parameter, and θ is the damping rate. Since $dB(t)$ is a white noise, it follows that

$$\langle x(t)x(t+\tau)\rangle = \int_0^{\infty} R(t')R(t'+\tau)\,dt' = \frac{\sigma^2}{2\theta}e^{-\theta\tau}, \qquad (12)$$

where the angle brackets throughout this paper denote ensemble averaging. Hence, the characteristic correlation time of an OU process is $\tau = 1/\theta$. In the multibox EBM with N vertically distributed boxes, the temperature $\Delta T_1(t)$ is given by

$$\Delta T_1(t) = \int_{-\infty}^{t}\left[\sum_{k=1}^{N} b_k e^{\lambda_k(t-s)}\right] d\Delta F(s) = \sum_{k=1}^{N} b_k \Delta T_{1,k}(t), \qquad (13)$$

where

$$\Delta T_{1,k}(t) = \int_{-\infty}^{t} e^{\lambda_k(t-s)}\,d\Delta F(s). \qquad (14)$$

If we consider the perturbations of the radiative forcing caused by volcanoes, solar variability, and anthropogenic activity as "deterministic," and the perturbations from the chaotic atmospheric dynamics as random, then it is natural to model the forcing as a superposition of a deterministic component and a white-noise random process:[1]

$$d\Delta F(t) = \Delta F_{\text{det}}(t)dt + \sigma dB(t).$$

Since the N-box models we consider are linear, the decomposition of the forcing yields a straightforward decomposition of the temperature response:

$$\begin{aligned}\Delta T_1(t) &= \Delta T_{1,\text{det}}(t) + \sigma\int_{-\infty}^{t}\left[\sum_{k=1}^{N} b_k e^{\lambda_k(t-s)}\right] dB(s)\\ &= \Delta T_{1,\text{det}}(t) + \sigma\sum_{k=1}^{N} b_k x_k(t),\end{aligned} \qquad (15)$$

where the processes

$$x_k(t) = \int_{-\infty}^{t} e^{\lambda_k(t-s)}\,dB(s)$$

are dependent OU processes with characteristic time scales given by the eigenvalues of the matrix $\mathbf{C}^{-1}\mathbf{K}$ via the relations $\tau_k = -1/\lambda_k$. Taking the Fourier transform of Eq. (14) yields

$$\Delta T_{1,k}(\omega) = \frac{\Delta F(\omega)}{i\omega + 1/\tau_k},$$

and the PSD of $\Delta T_1(t)$ becomes

$$\begin{aligned}S_1(\omega) &= \lim_{T\to\infty}\frac{1}{T}\langle|\Delta T_1(\omega)|^2\rangle\\ &= \lim_{T\to\infty}\frac{1}{T}\langle|\Delta F(\omega)|^2\rangle[S^{(0)}(\omega) + S^{(\text{cr})}(\omega)],\end{aligned}$$

where

$$\begin{aligned}S^{(0)}(\omega) &= \sum_k \frac{b_k^2}{(\omega_k^2 + \omega^2)},\\ S^{(\text{cr})}(\omega) &= \sum_k\sum_{j<k}\frac{2b_kb_j(\omega_k\omega_j + \omega^2)}{(\omega_j^2+\omega^2)(\omega_k^2+\omega^2)}, \quad \text{and} \quad \omega_k = 1/\tau_k.\end{aligned} \qquad (16)$$

[1] In this paper, we follow Rypdal and Rypdal (2014) and model the random component of the forcing as white noise. However, the models can easily be modified to other stochastic models for the random forcing.

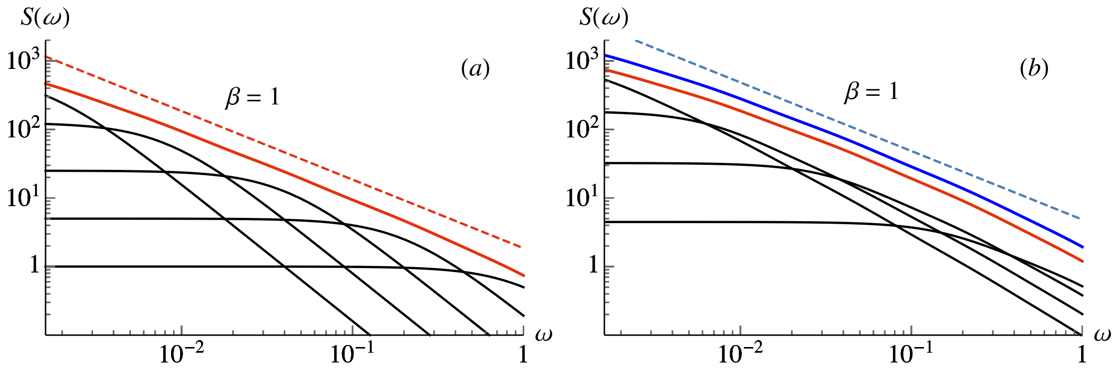

FIG. 1. (a) The solid red line shows the sum $S^{(0)}(\omega)$ in Eq. (16), with $N = 5, \beta = 1, \tau_1 = 1, b_1 = 1$, and $a = 5$. The dashed red line shows a power law of $1/f^\beta$, with $\beta = 1$. The black lines show the contribution from each term in the aggregation. (b) The red line shows the sum $S^{(\mathrm{cr})}(\omega)$, while the blue line shows $S^{(0)}(\omega) + S^{(\mathrm{cr})}(\omega)$. The dashed blue line shows the power-law spectrum we approximate, given the same forcing for all modes. The black lines show the contribution to $S^{(\mathrm{cr})}(\omega)$ for each k: $\sum_{j<k} 2b_k b_j(\omega_k\omega_j + \omega^2)[(\omega_j^2 + \omega^2)(\omega_k^2 + \omega^2)]^{-1}$.

Here, T is the length of the time series $\Delta T_1(t)$, $S^{(0)}(\omega)$ is the PSD of an independent superposition of the processes $\Delta T_{1,k}(t)$, and $S^{(\mathrm{cr})}(\omega)$ is the contribution to the PSD from the cross terms, which cannot be neglected since the processes $\Delta T_{1,k}(t)$ are driven by the same forcing $\Delta F(t)$. For the stochastic component of the process Eq. (15), we can replace the forcing by a white noise process such that $\lim_{T\to\infty} T^{-1}\langle|\Delta F(\omega)|^2\rangle$ is a constant in ω.

Before we proceed to estimating parameters from data, we demonstrate that the PSD in Eq. (16) can easily be made to approximate a power law. For instance, can we pick time scales τ_k such that $\tau_{k+1} = a\tau_k$ and weights b_k such that $b_{k+1} = \sqrt{a^{\beta-2}}b_k$. Then we have the approximate relations $S^{(0)}(\omega) \sim \omega^\beta$, $S^{(\mathrm{cr})}(\omega) \sim \omega^\beta$, and hence $S_1(\omega) \sim \omega^\beta$. In Fig. 1, this is demonstrated for a superposition of $N = 5$ terms. The sum $S^{(0)}(\omega)$ is shown by the red line in Fig. 1a and the total sum $S^{(0)}(\omega) + S^{(\mathrm{cr})}(\omega)$ by the blue line in Fig. 1b. The idea that a long memory process can be produced by aggregating OU processes is the same as presented by, for example, Granger (1980) and M. Rypdal (2016). In this paper, the time scales τ_k and their weights b_k are estimated from data without a priori assumptions of scale invariance.

a. Example 1: The two-box model

For the classical two-box model, Geoffroy et al. (2013) estimated parameters by fitting the GMST response in the two-box model to the corresponding response in CMIP5 models. The forcing scenario used for fitting was abrupt quadrupling of atmospheric CO_2 concentration. They find multimodel mean parameter estimates $\hat{C}_1 = 7.3\,\mathrm{W\,yr\,m^{-2}\,K^{-1}}$, $\hat{C}_2 = 106\,\mathrm{W\,yr\,m^{-2}\,K^{-1}}$, $\hat{\kappa}_1 = 1.13\,\mathrm{W\,m^{-2}\,K^{-1}}$, and $\hat{\kappa}_2 = 0.73\,\mathrm{W\,m^{-2}\,K^{-1}}$, which correspond to characteristic time scales of 3.88 and 242 yr. The two-box model provides a good fit to CMIP5 abrupt $4\times CO_2$ experiments and $1\%\,\mathrm{yr^{-1}}$ CO_2 increase experiments over 140 years, but, if forced with white noise, the PSD is $S_1(\omega) \propto S^{(0)}(\omega) + S^{(\mathrm{cr})}(\omega)$. Using the parameters estimated by Geoffroy et al. (2013) for three different CMIP5 models, we have plotted this expression in Fig. 2a. As seen from Fig. 2, the PSD can be approximated by two different power laws: one in the high-frequency range and another in the low-frequency range. For frequencies corresponding to time scales greater than a few decades, the PSD can be approximated by $S(f) \propto 1/f^\beta$, with $\beta = 0.3$, and for the higher frequencies it can be approximated by $S(f) \propto 1/f^2$. This result is inconsistent with the PSDs estimated from CMIP5 control run temperatures, which are well approximated by one power law over the entire range of frequencies from months to centuries (Fredriksen and Rypdal 2016).

The inability of the two-box model to simultaneously describe the average GMST response to certain forcing scenarios in GCMs, as well as the PSD of the background fluctuations, serves as a motivation to analyze more general N-box models, and in the next example we consider the EBM with three vertically distributed boxes. We will demonstrate that the three-box model provides accurate descriptions of both the deterministic response to historic radiative forcing and the statistical properties of the response to random forcing.

b. Example 2: The three-box model

The three-box model is given by Eq. (6) with

$$\mathbf{C} = \begin{bmatrix} C_1 & 0 & 0 \\ 0 & C_2 & 0 \\ 0 & 0 & C_3 \end{bmatrix}, \quad \Delta\mathbf{T} = \begin{bmatrix} \Delta T_1 \\ \Delta T_2 \\ \Delta T_3 \end{bmatrix}, \quad \text{and}$$

$$\Delta\mathbf{F}(t) = \begin{bmatrix} \Delta F(t) \\ 0 \\ 0 \end{bmatrix}$$

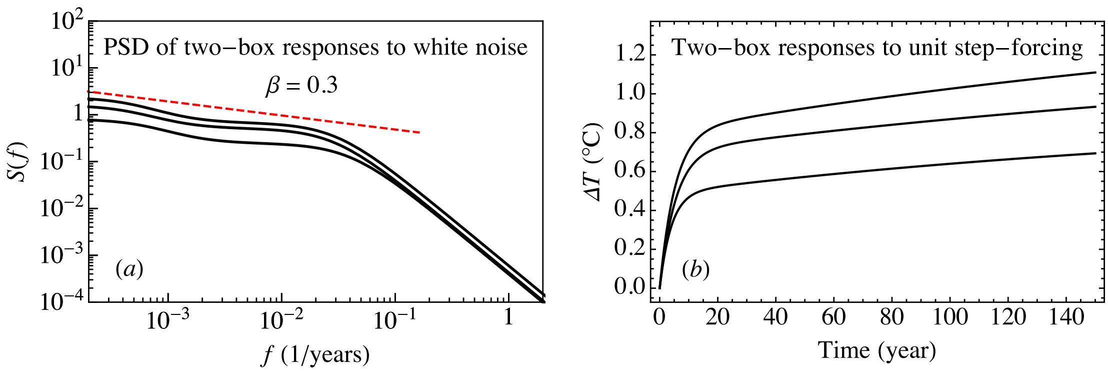

FIG. 2. (a) Theoretical PSD of the response to white-noise forcing for a two-box model, with three different sets of parameters. The dashed red line shows a power law $1/f^{\beta}$, with $\beta = 0.3$ for reference. (b) The response to a unit step forcing for the same parameter choices. The three different sets of parameter choices are those estimated by Geoffroy et al. (2013) from the following models: HadGEM2-ES: $(\kappa_1, \kappa_2) = (0.65, 0.55)$ W m^{-2} K^{-1} and $(C_1, C_2) = (6.5, 82)$ W yr m^{-2} K^{-1}, IPSL-CM5A-LR: $(\kappa_1, \kappa_2) = (0.79, 0.59)$ W m^{-2} K^{-1} and $(C_1, C_2) = (7.7, 95)$ W yr m^{-2} K^{-1}, and NorESM1-M: $(\kappa_1, \kappa_2) = (1.11, 0.88)$ W m^{-2} K^{-1} and $(C_1, C_2) = (8.0, 105)$ W yr m^{-2} K^{-1}.

and

$$\mathbf{K} = \begin{bmatrix} -(\kappa_1 + \kappa_2) & \kappa_2 & 0 \\ \kappa_2 & -(\kappa_2 + \kappa_3) & \kappa_3 \\ 0 & \kappa_3 & -\kappa_3 \end{bmatrix}. \qquad (17)$$

To estimate the parameters in the model, we will make use of the HadCRUT4 dataset for the GMST since 1850 (Morice et al. 2012) and the global effective forcing data, both with annual resolution. The forcing data is an updated version of Hansen et al. (2011) (available at http://www.columbia.edu/~mhs119/Forcings/). We also use the Moberg Northern Hemisphere temperature reconstruction (Moberg et al. 2005) and the Crowley forcing data (Crowley 2000) for the years 1000–1979. We fix a set of three well separated time scales (τ_1, τ_2, and τ_3) and compute the responses

$$\Delta T_{1,k}(t) = \int_{t_0}^{t} e^{-(t-s)/\tau_k} \Delta F(s)\, ds, \quad \text{for} \quad k = 1, 2, \text{ and } 3,$$

to the historical forcing data $\Delta F(t)$, where the integral is estimated by a sum. As in Eq. (13), the GMST response is a linear combination of the responses $\Delta T_{1,k}(t)$:

$$\Delta T_1(t) = b_1 \Delta T_{1,1}(t) + b_2 \Delta T_{1,2}(t) + b_3 \Delta T_{1,3}(t),$$

and our approach is to estimate the parameters b_1, b_2, and b_3 from historical data of GMST and forcing. We will subsequently demonstrate that, for the range of time scales we consider in this paper, the results are largely insensitive to the choice of time scales (τ_1, τ_2, and τ_3), as long as these are sufficiently separated. We do not only require that the deterministic response to radiative forcing fits well with observations, but also that the PSD of the stochastic component of the response is consistent with the estimated PSD of the residual observational signal (the difference between observed temperature record and the model response to the deterministic forcing). Rypdal and Rypdal (2014) employ a maximum-likelihood method to estimate the variance of the temperature residual σ_T^2 and the spectral exponent β of a long-memory model. This method is inadequate here, since we have more free parameters and the method favors a good fit for the smallest time scales.

We employ instead an iterative routine, which in addition to weighting all the time scales in the estimation, allows us to fit to a composite spectrum. We first compute the residual temperature by guessing the model parameters, computing the deterministic responses to the Crowley and Hansen forcing time series, and then subtracting the deterministic responses from the observed Moberg temperature and HadCRUT4 records. The PSD of the residual is estimated using the periodogram and subsequently log binned. The theoretical PSD of the response to white-noise forcing in the three-box model is then fitted to the composite residual PSD derived from the temperatures from Moberg and HadCRUT4 by minimizing the square distance between the theoretical and estimated residual PSDs. From this, we obtain new estimates of the relative size of the weights b_k at each time scale, and using these we perform a new regression analysis with HadCRUT4 to determine the initial temperature T_0 and the absolute strength of the response. The procedure is repeated with these new model parameters as a starting point. The parameter estimation converges rapidly; only a few iterations are needed to obtain our estimates.

In Figs. 3a,c, we show the deterministic responses to historical forcing with estimated parameters. The three

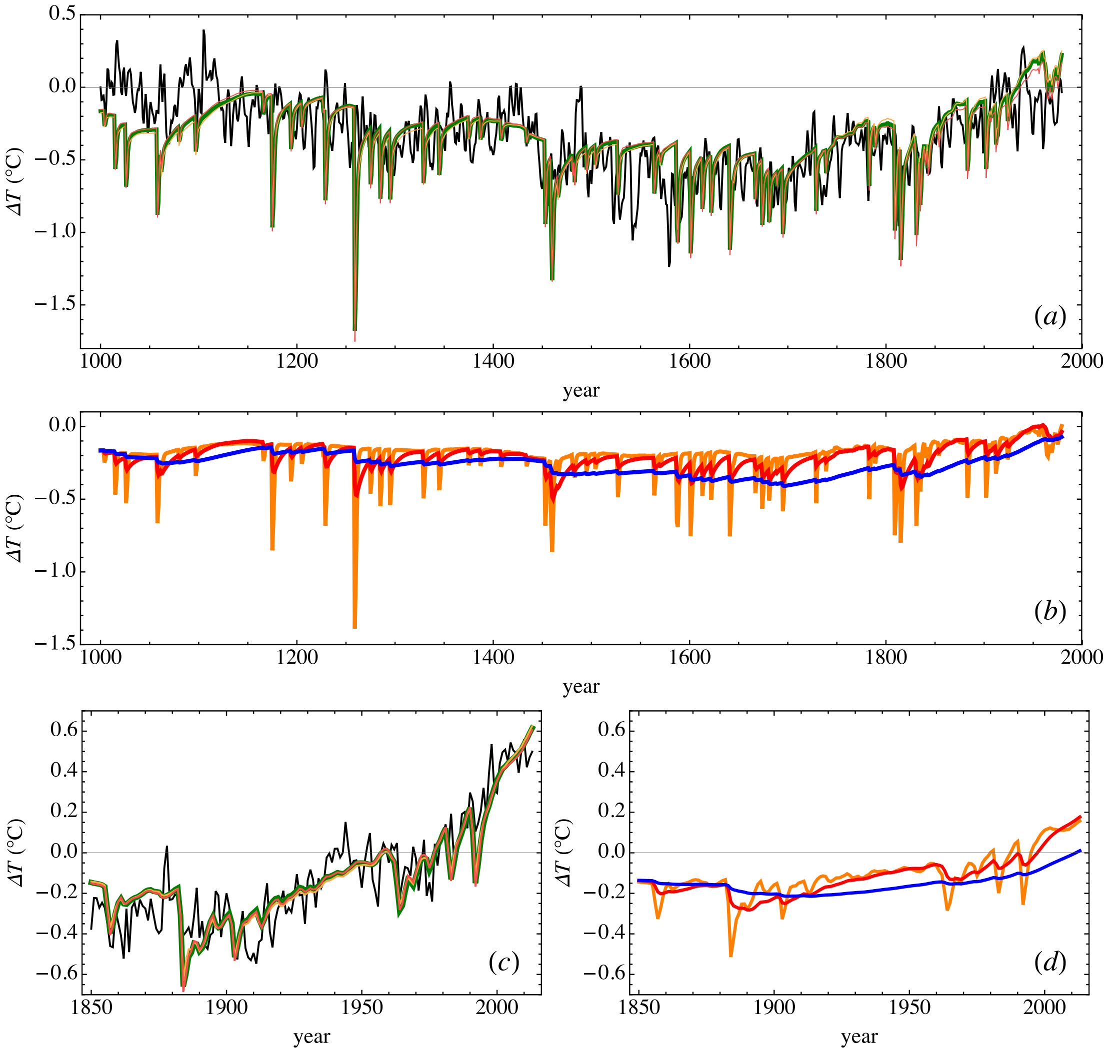

FIG. 3. (a) The black curve is the Moberg temperature reconstruction, and the colored curves are the responses to Crowley forcing of the three-box model with estimated parameters. The orange curve is the response of the three-box model where we have fixed time scales $\tau_1 = 0.5$ yr, $\tau_2 = 5$ yr, and $\tau_3 = 50$ yr. The thicker green curve is the response of the three-box model where we have fixed time scales $\tau_1 = 1$ yr, $\tau_2 = 10$ yr, and $\tau_3 = 100$ yr. The red curve is the response of the three-box model where we have fixed time scales $\tau_1 = 1$ yr, $\tau_2 = 20$ yr, and $\tau_3 = 400$ yr. (c) As in (a), but showing the response to forcing over the instrumental period, and the black curve is the global instrumental temperature from HadCRUT4. (b),(d) The green curves in (a) and (c) decomposed into the responses corresponding to the exponential terms in the response function $R(t)$. The orange curve corresponds to $\tau_1 = 1$ yr, the red curve corresponds to $\tau_2 = 10$ yr, and the blue curve corresponds to $\tau_3 = 100$ yr.

different colors represent different choices of the time scales τ_1, τ_2, and τ_3, and the parameter estimates are presented in Table 1, where we also present the corresponding values of the parameters κ_k and C_k, as well as the equilibrium climate sensitivity of the model. We note that the colored curves in Figs. 3a,c are almost indistinguishable, and they all closely follow the HadCRUT4 and Moberg records.

Figure 4a shows the theoretical PSD of the stochastic component (the response to white-noise forcing) in the model. The estimated parameters are shown in Table 1, and the choice of time scales are $\tau_1 = 1$ yr, $\tau_2 = 10$ yr, and $\tau_3 = 100$ yr. The PSD of the model fits well with the PSD estimated from observational data in the time-scale range from months to centuries, and in this range it is close to a power law with an exponent $\beta = 0.65$.

In Fig. 4b, we show the three-box model responses to a unit step-forcing scenario. The different colors correspond to different choices of the time scales τ_1, τ_2, and τ_3, and the gray curves are the corresponding two-box model responses with parameters estimated by Geoffroy et al. (2013) by fitting to abrupt 4 × CO_2 experiments in CMIP5 models. From the response to a unit step forcing, we can also derive that the equilibrium

TABLE 1. Parameters estimated from data. The time scales τ_k and their weights b_k for $k = 1, 2$, and 3 uniquely determine the estimated response functions. The parameter $\sigma_{\mathrm{monthly}}$ is the estimated standard deviation of the monthly resolved stochastic forcing. The values for $T_{0,\mathrm{instr}}$ and $T_{0,\mathrm{Moberg}}$ are the initial temperature anomalies estimated for global instrumental temperature and the Moberg temperature reconstruction. We note that there is some remnant seasonal variability that we were not able to remove by subtracting a mean seasonal cycle. This is not so apparent in a double-logarithmic plot of the PSD, but it causes our estimates of $\sigma_{\mathrm{monthly}}$ to be slightly inconsistent with the actual residual variability. We also point out that our estimates of $\sigma_{\mathrm{monthly}}$ are only valid for monthly resolved temperatures, or monthly temperatures sampled at a different time resolution.

	Time scales (τ_1, τ_2, τ_3) (yr)		
Parameter (units)	(0.5, 5, 50)	(1, 10, 100)	(1, 20, 400)
b_1 ($\mathrm{K\,m^2\,W^{-1}\,yr^{-1}}$)	0.198	0.165	0.187
b_2 ($\mathrm{K\,m^2\,W^{-1}\,yr^{-1}}$)	0.033	0.022	0.018
b_3 ($\mathrm{K\,m^2\,W^{-1}\,yr^{-1}}$)	0.011	0.005	0.001
$\sigma_{\mathrm{monthly}}$ ($\mathrm{W\,m^{-2}\,yr^{-1/2}}$)	0.73	0.70	0.68
$T_{0,\mathrm{instr}}$ (K)	−0.13	−0.14	−0.14
$T_{0,\mathrm{Moberg}}$ (K)	−0.18	−0.17	−0.15
S_{eq} ($\mathrm{K\,m^2\,W^{-1}}$)	0.79	0.85	1.07
C_1 ($\mathrm{W\,yr\,m^{-2}\,K^{-1}}$)	4.15	5.09	4.86
C_2 ($\mathrm{W\,yr\,m^{-2}\,K^{-1}}$)	15.4	22.0	31.7
C_3 ($\mathrm{W\,yr\,m^{-2}\,K^{-1}}$)	24.1	41.8	149
κ_1 ($\mathrm{W\,m^{-2}\,K^{-1}}$)	1.26	1.18	0.94
κ_2 ($\mathrm{W\,m^{-2}\,K^{-1}}$)	5.61	3.30	3.50
κ_3 ($\mathrm{W\,m^{-2}\,K^{-1}}$)	1.74	1.2	0.91

climate sensitivity for an N-box model is given by $S_{\mathrm{eq}} = \sum_{k=1}^{N} b_k \tau_k$.

The difference we observe in the step-forcing responses is not a result of a difference between the two- and three-box models, but rather a difference in estimation strategy. In our estimation procedure, we use only observational and proxy data and have hence chosen the parameters that best reproduce both the residual spectra and responses to historical forcing. The parameters estimated by this method are not the same as the parameters that best describe the $4 \times CO_2$ runs. This discrepancy can have several explanations; perhaps is the random forcing not accurately modeled as a white noise, or the forcing in the $4 \times CO_2$ experiments is too strong for a linear approximation to be valid. It is likely that the feedback parameter or parameters related to ocean mixing can change during the strong and abrupt climate change following a quadrupling in CO_2 concentration. The large differences between the different CMIP5 step responses also reflect the large uncertainty associated with these model runs.

c. *Example 3: Separate boxes for land and ocean*

With two surface boxes, one for land and one for ocean, the equation for the ocean surface temperature is

$$C_1 \frac{d}{dt}\Delta T_1 = -\kappa_1' \Delta T_1 + F_N + F_O(t) + \frac{k}{f_O(\lambda_L + k/f_L)} F_L(t), \tag{18}$$

where

$$\kappa_1' = \lambda_O + k\mu\alpha/f_O - \frac{k^2 \mu\alpha}{f_O f_L(\lambda_L + k/f_L)}. \tag{19}$$

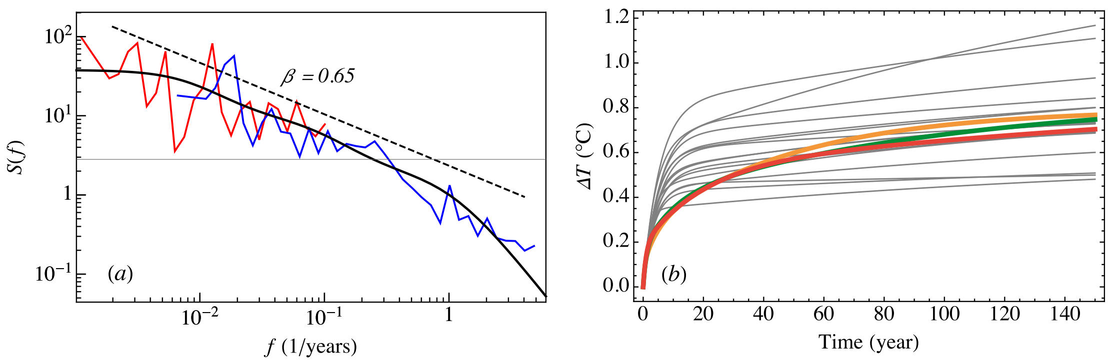

FIG. 4. (a) The blue curve is the estimated PSD of the residual global instrumental temperature after subtracting the estimated deterministic response of a three-box model. The characteristic time scales in the three-box model are chosen to be $\tau_1 = 1$ yr, $\tau_2 = 10$ yr, and $\tau_3 = 100$ yr. The red curve is the residual of the Moberg temperature reconstruction. Both curves are normalized by their power on decadal scales. The black curve is the theoretical PSD with the estimated response function, which can be quite well approximated by a power law, shown by the dashed line with slope $-\beta = 0.65$. (b) The gray curves are the responses to a unit step forcing using two-box model parameters estimated for many climate models by Geoffroy et al. (2013). The colored curves show the three-box responses with the parameters from Table 1. The orange curve is the response of the three-box model where we have fixed time scales $\tau_1 = 0.5$ yr, $\tau_2 = 5$ yr, and $\tau_3 = 50$ yr. The thicker green curve is the response of the three-box model where we have fixed time scales $\tau_1 = 1$ yr, $\tau_2 = 10$ yr, and $\tau_3 = 100$ yr. The red curve is the response of the three-box model where we have fixed time scales $\tau_1 = 1$ yr, $\tau_2 = 20$ yr, and $\tau_3 = 400$ yr.

TABLE 2. Parameters estimated from global sea and land surface temperatures. The fixed time scales are chosen to be $\tau_1 = 0.5$ yr, $\tau_2 = 5$ yr, and $\tau_3 = 50$ yr.

Sea		Land	
b_1	$0.092\,\mathrm{K\,m^2\,W^{-1}\,yr^{-1}}$	r_1	$0.10\,\mathrm{K\,m^2\,W^{-1}}$
b_2	$0.035\,\mathrm{K\,m^2\,W^{-1}\,yr^{-1}}$	r_2	1.40
b_3	$0.009\,\mathrm{K\,m^2\,W^{-1}\,yr^{-1}}$	—	—
$\sigma_{\mathrm{monthly,sea}}$	$0.76\,\mathrm{W\,m^{-2}\,yr^{-1/2}}$	$\sigma_{\mathrm{monthly,land}}$	$0.2\,\mathrm{W\,m^{-2}\,yr^{-1/2}}$
$T_{0,\mathrm{sea}}$	-0.13 K	$T_{0,\mathrm{land}}$	-0.15 K
$S_{\mathrm{eq,sea}}$	$0.69\,\mathrm{K\,m^2\,W^{-1}}$	$S_{\mathrm{eq,land}}$	$1.07\,\mathrm{K\,m^2\,W^{-1}}$

The response function can hence be estimated in the same way as for global temperature, and the results are given in Table 2. For the estimation, we have used the global Hadley Centre SST, version 3 (HadSST3; Kennedy et al. 2011a,b), dataset.

Simplifying the constants in Eq. (10), and separating the stochastic (stoc) and deterministic (det) parts results in

$$\Delta T_L(t) = r_1 F_L(t) + r_2 \Delta T_1 = r_1 F_{L,\mathrm{det}}(t) + r_2 \Delta T_{1,\mathrm{det}}(t) + r_1 \sigma_L dB_L(t) + r_2 \Delta T_{1,\mathrm{stoc}}(t), \tag{20}$$

where $\sigma_L dB_L(t)$ is the direct stochastic forcing of the land surface temperature. For the ocean response, we use the previously estimated parameters, given in Table 2. The remaining parameters are chosen such that the deterministic response

$$\Delta T_{L,\mathrm{det}} = T_0 + r_1 F_{L,\mathrm{det}} + r_2 \Delta T_{1,\mathrm{det}} \tag{21}$$

is similar to global land surface temperature (LST) and such that the PSD of the residual temperature obtained after subtracting the deterministic response is similar to the PSD expected for the stochastic part of Eq. (20):

$$\langle |\Delta T_{L,\mathrm{stoc}}(\omega)|^2 \rangle = (r_1 \sigma_L)^2 \Delta t + r_2^2 \langle |\Delta T_{1,\mathrm{stoc}}(\omega)|^2 \rangle. \tag{22}$$

Here we assume that the instantaneous response in ocean temperature to changes in the direct forcing of the land temperature is small compared to the land temperature response to this forcing. For the global LST, we use the Climatic Research Unit (CRU) land air temperature, version 4 variance adjusted (CRUTEM4v; Jones et al. 2012), dataset. The observed SST, LST, and the response to deterministic forcing with the parameters listed in Table 2 are shown in Fig. 5. Figure 5 also shows the estimated and theoretical PSD of the response to stochastic forcing with the same parameters. The global temperature response $\Delta T_G = f_L \Delta T_L + f_O \Delta T_1$ is similar to the three-box temperature response estimated directly from global temperature.

The theoretical PSD of $\Delta T_1(t)$ fits well with the estimated PSD of the SST residual, and both are well approximated by a power law with $\beta_O \approx 1$. In the same way, the theoretical PSD of $\Delta T_L(t)$ fits well with the estimated PSD of the LST, and both can be approximated by a power law with $\beta_L \approx 0.5$. These results are similar to the estimated PSDs of the linearly detrended global LST and global SST analyzed in Fredriksen and Rypdal (2016). With this model, the only reason global LST shows persistence is because of the influence by global SST, but the persistence is weaker for land than for sea as a result of the component responding instantly to forcing.

We note that, in the model presented in this paper, the relation between the equilibrium climate sensitivities for land temperatures and ocean temperatures is

$$S_{\mathrm{eq,land}} = r_1 + r_2 S_{\mathrm{eq,sea}}.$$

If $r_1/r_2 \ll S_{\mathrm{eq,sea}}$, there will be a near-constant ratio between land and ocean temperature change, consistent with the findings of Lambert et al. (2011).

4. Discussion and conclusions

Simple climate models can be divided in two classes: EBMs and tuned impulse–response (IR) linear statistical models (Good et al. 2011). The power-law response model proposed by Rypdal and Rypdal (2014) is an example of an IR model that reproduces observed temperature variability quite well, but in this mathematical idealization conservation of energy is lost. It may also be unclear what the physical reason for using this model is. In this paper, we demonstrate that such a model is closely approximated by the response of a multibox EBM. This shows that LRD models can be seen as a compact mathematical description of the effect of a range of time scales in the physical response.

Linear EBMs have been studied since Budyko (1969) and Sellers (1969), with various models for how the heat is taken up by the ocean. Many of them include also an additive stochastic forcing, assumed to be generated by a

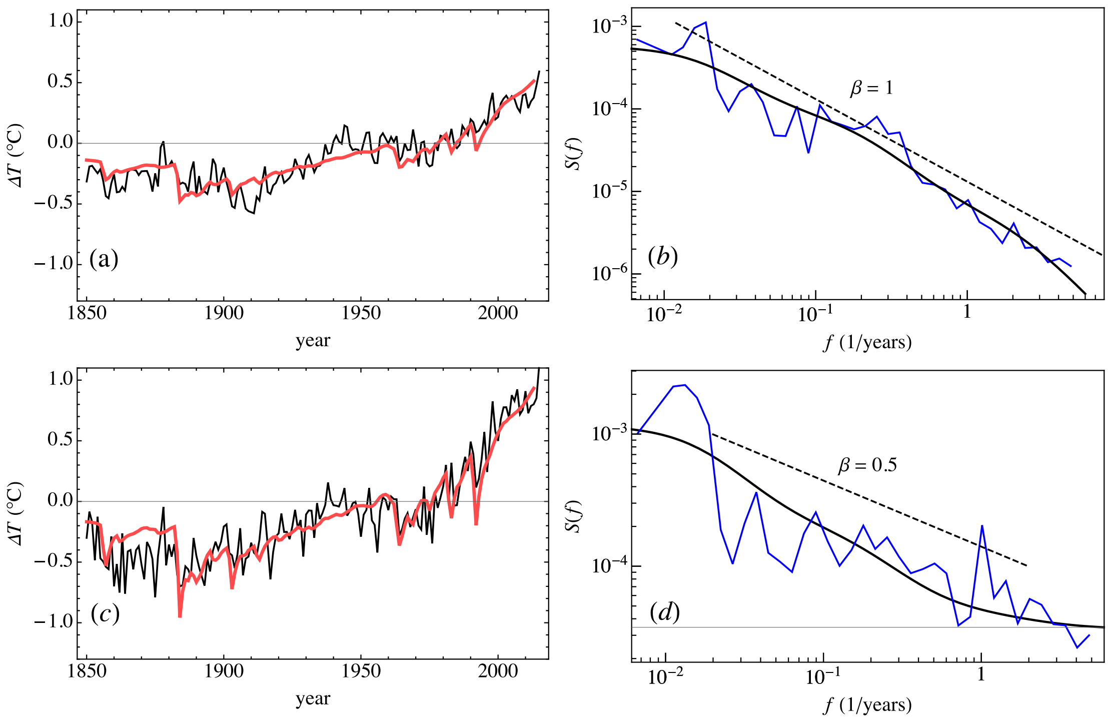

FIG. 5. (a) The black curve is the global HadSST3 dataset, and the red curve is the response to forcing on time scales of 0.5, 5, and 50 yr. (b) The blue curve is the spectrum of the residual of HadSST3 after subtracting the red curve in (a), and the black curve is the expected spectrum of the residual. The dashed black line shows a power law $1/f^{\beta}$ for reference. (c),(d) As in (a),(b), but for the global CRUTEM4v dataset. In addition to the three time scales, we have an instantaneous response to the forcing for land temperatures.

truncation of the dynamics on shorter scales than the response (Hasselmann 1976). Weather systems and day-to-day variations in insolation and outgoing radiation due to variations in cloud cover are likely important parts of the noisy forcing. These are known to be unpredictable on the scales of the climate response, and a Gaussian white noise description in time may be reasonable.

The ocean then integrates the forcing on several time scales, but it is difficult to point out exactly what the time scales are. The reason is that the response appears to be practically indistinguishable from a power law, even if we do not assume this a priori. By picking a set of time scales that is sufficiently separated within the range of the scales where we expect a climate response, we obtain a set of sufficiently different predictors to describe global temperature evolution. We find that three time scales is the least number needed to approximate the temperature response. The resulting description of global temperature in terms of this set of predictors should be seen as a statistical model with a minimal number of parameters to be estimated from data—a model that can also be replaced by a simpler power-law response with even fewer parameters to estimate.

Contrary to the power-law response, the response derived from the EBM has a physical fundament of energy conservation and some description of energy exchange within the system. Even though the model is oversimplified, the power-law-shaped spectrum we obtain for global surface temperature with this simple model is consistent with the slightly more advanced linear diffusion models, where Fraedrich et al. (2004) and Lemke (1977) report $1/f$ noise characteristics, as well as with the power-law spectra observed in complex GCMs (Fredriksen and Rypdal 2016). It is difficult to draw any general conclusions about the physical parameters in the simple model from the large separation of time scales, since each time scale and corresponding response depends on all parameters in the linear model. One general feature for our estimated parameters is that $C_1 < C_2 < C_3$, but the large separation of time scales does not necessarily imply that the heat capacities must be well separated.

The EBMs considered in this paper consist only of one or two surface boxes and can therefore only describe the correlation structure of global temperature in time. Several papers consider EBMs extended to describe a horizontal temperature field (North and Cahalan 1981; Kim and North 1991; North et al. 2011). These models were expanded to include a simple model for ocean diffusion and upwelling by Kim and North (1992) and were compared to early versions of GCMs by Kim et al. (1996). More recently, work on two-dimensional stochastic–diffusive EBMs by North et al. (2011) was generalized to include long-memory temporal response by Rypdal et al. (2015). An important result derived from this generalization is power-law spectra for both local and global temperature, and spectral exponent of global temperature, which is twice that of local temperatures, are in good agreement with observations. The spatial model proposed by Rypdal et al. (2015) could be approximated by a sum of spatial fields with AR(1) characteristics in time, similar to our approximation for global temperature in this paper.

As suggested by Ragone et al. (2016), we believe that the global temperature response in the Holocene can be well approximated as linear. Extending the linear response to local and regional temperatures is more problematic, especially for the temperature responses in the Arctic, where strong nonlinear effects such as the sea ice–albedo feedback are present. Despite this, linear responses as in Lucarini et al. (2017) or derived from spatially dependent EBMs have considerable success in describing most local temperatures. The multibox models can also easily be extended to include nonlinear terms: for instance, to describe the rapid sea ice loss in the Arctic. And they can be extended to include different types of tipping points, which allows us to study critical transitions in systems that exhibit LRD. The effect of LRD on the early warning indicators associated with critical transitions in multibox EMBs is a topic that will be pursued in future work.

Acknowledgments. The authors thank K. Rypdal and O. Løvsletten for useful discussions. The paper was supported by the Norwegian Research Council (KLIMAFORSK Programme) under Grant 229754.

REFERENCES

Armour, K. C., C. M. Bitz, and G. H. Roe, 2013: Time-varying climate sensitivity from regional feedbacks. *J. Climate*, **26**, 4518–4534, doi:10.1175/JCLI-D-12-00544.1.

Benestad, R. E., D. Nuccitelli, S. Lewandowsky, K. Hayhoe, H. O. Hygen, R. van Dorland, and J. Cook, 2016: Learning from mistakes in climate research. *Theor. Appl. Climatol.*, **126**, 699–703, doi:10.1007/s00704-015-1597-5.

Blender, R., K. Fraedrich, and B. Hunt, 2006: Millennial climate variability: GCM simulation and Greenland ice cores. *Geophys. Res. Lett.*, **33**, L04710, doi:10.1029/2005GL024919.

Budyko, M. I., 1969: The effect of solar radiation variations on the climate of the Earth. *Tellus*, **21**, 611–619, doi:10.3402/tellusa.v21i5.10109.

Caldeira, K., and N. P. Myhrvold, 2013: Projections of the pace of warming following an abrupt increase in atmospheric carbon dioxide concentration. *Environ. Res. Lett.*, **8**, 034039, doi:10.1088/1748-9326/8/3/034039.

Cohn, T. A., and H. F. Lins, 2005: Nature's style: Naturally trendy. *Geophys. Res. Lett.*, **32**, L23402, doi:10.1029/2005GL024476.

Crowley, T. J., 2000: Causes of climate change over the past 1000 years. *Science*, **289**, 270–277, doi:10.1126/science.289.5477.270.

Fraedrich, K., 2002: Fickian diffusion and Newtonian cooling: A concept for noise induced climate variability with long-term memory? *Stochastic Dyn.*, **2**, 403–412, doi:10.1142/S0219493702000492.

——, and R. Blender, 2003: Scaling of atmosphere and ocean temperature correlations in observations and climate models. *Phys. Rev. Lett.*, **90**, 108501, doi:10.1103/PhysRevLett.90.108501.

——, U. Luksch, and R. Blender, 2004: 1/f model for long-time memory of the ocean surface temperature. *Phys. Rev.*, **70E**, 037301, doi:10.1103/PhysRevE.70.037301.

Franzke, C., 2010: Long-range dependence and climate noise characteristics of Antarctic temperature data. *J. Climate*, **23**, 6074–6081, doi:10.1175/2010JCLI3654.1.

——, S. M. Osprey, P. Davini, and N. W. Watkins, 2015: A dynamical systems explanation of the Hurst effect and atmospheric low-frequency variability. *Sci. Rep.*, **5**, 9068, doi:10.1038/srep09068.

Fredriksen, H.-B., and K. Rypdal, 2016: Spectral characteristics of instrumental and climate model surface temperatures. *J. Climate*, **29**, 1253–1268, doi:10.1175/JCLI-D-15-0457.1.

Geoffroy, O., D. Saint-Martin, D. J. L. Olivié, A. Voldoire, G. Bellon, and S. Tytéca, 2013: Transient climate response in a two-layer energy-balance model. Part I: Analytical solution and parameter calibration using CMIP5 AOGCM experiments. *J. Climate*, **26**, 1841–1857, doi:10.1175/JCLI-D-12-00195.1.

Good, P., J. M. Gregory, and J. A. Lowe, 2011: A step-response simple climate model to reconstruct and interpret AOGCM projections. *Geophys. Res. Lett.*, **38**, L01703, doi:10.1029/2010GL045208.

Granger, C. W. J., 1980: Long memory relationships and the aggregation of dynamic models. *J. Econ.*, **14**, 227–238, doi:10.1016/0304-4076(80)90092-5.

Hansen, J., M. Sato, P. Kharecha, and K. von Schuckmann, 2011: Earth's energy imbalance and implications. *Atmos. Chem. Phys.*, **11**, 13 421–13 449, doi:10.5194/acp-11-13421-2011.

Hasselmann, K., 1976: Stochastic climate models. Part 1. Theory. *Tellus*, **6**, 473–485.

Held, I. M., M. Winton, K. Takahashi, T. Delworth, F. Zeng, and G. K. Vallis, 2010: Probing the fast and slow components of global warming by returning abruptly to preindustrial forcing. *J. Climate*, **23**, 2418–2427, doi:10.1175/2009JCLI3466.1.

Huybers, P., and W. Curry, 2006: Links between annual, Milankovitch and continuum temperature variability. *Nature*, **441**, 329–332, doi:10.1038/nature04745.

Jones, P. D., D. H. Lister, T. J. Osborn, C. Harpham, M. Salmon, and C. P. Morice, 2012: Hemispheric and large-scale land-surface air temperature variations: An extensive revision and an update to 2010. *J. Geophys. Res.*, **117**, D05127, doi:10.1029/2011JD017139.

Kennedy, J. J., N. A. Rayner, R. O. Smith, D. E. Parker, and M. Saunby, 2011a: Reassessing biases and other uncertainties in sea surface temperature observations measured in situ since 1850: 1. Measurement and sampling uncertainties. *J. Geophys. Res.*, **116**, D14103, doi:10.1029/2010JD015218.

——, ——, ——, ——, and ——, 2011b: Reassessing biases and other uncertainties in sea surface temperature observations measured in situ since 1850: 2. Biases and homogenization. *J. Geophys. Res.*, **116**, D14104, doi:10.1029/2010JD015220.

Kim, K.-Y., and G. R. North, 1991: Surface temperature fluctuations in a stochastic climate model. *J. Geophys. Res.*, **96**, 18 573–18 580, doi:10.1029/91JD01959.

——, and ——, 1992: Seasonal cycle and second-moment statistics of a simple coupled climate system. *J. Geophys. Res.*, **97**, 20 437–20 448, doi:10.1029/92JD02281.

——, ——, and G. C. Hegerl, 1996: Comparisons of the second-moment statistics of climate models. *J. Climate*, **9**, 2204–2221, doi:10.1175/1520-0442(1996)009<2204:COTSMS>2.0.CO;2.

Lambert, F. H., M. J. Webb, and M. M. Joshi, 2011: The relationship between land–ocean surface temperature contrast and radiative forcing. *J. Climate*, **24**, 3239–3256, doi:10.1175/2011JCLI3893.1.

Lemke, P., 1977: Stochastic climate models. Part 3. Application to zonally averaged energy models. *Tellus*, **29**, 385–392, doi:10.3402/tellusa.v29i5.11371.

Lovejoy, S., 2015: A voyage through scales, a missing quadrillion and why the climate is not what you expect. *Climate Dyn.*, **44**, 3187–3210, doi:10.1007/s00382-014-2324-0.

——, and D. Schertzer, 2013: *The Weather and Climate: Emergent Laws and Multifractal Cascades*. Cambridge University Press, 505 pp.

Lucarini, V., F. Ragone, and F. Lunkeit, 2017: Predicting climate change using response theory: Global averages and spatial patterns. *J. Stat. Phys.*, **166**, 1036–1064, doi:10.1007/s10955-016-1506-z.

Mann, M. E., 2011: On long range dependence in global surface temperature series. *Climatic Change*, **107**, 267–276, doi:10.1007/s10584-010-9998-z.

Meinshausen, M., S. C. B. Raper, and T. M. L. Wigley, 2011: Emulating coupled atmosphere–ocean and carbon cycle models with a simpler model, MAGICC6—Part 1: Model description and calibration. *Atmos. Chem. Phys.*, **11**, 1417–1456, doi:10.5194/acp-11-1417-2011.

Moberg, A., D. M. Sonechkin, K. Holmgren, N. M. Datsenko, and W. Karlén, 2005: Highly variable Northern Hemisphere temperatures reconstructed from low- and high-resolution proxy data. *Nature*, **433**, 613–617, doi:10.1038/nature03265.

Morice, C. P., J. J. Kennedy, N. A. Rayner, and P. D. Jones, 2012: Quantifying uncertainties in global and regional temperature change using an ensemble of observational estimates: The HadCRUT4 data set. *J. Geophys. Res.*, **117**, D08101, doi:10.1029/2011JD017187.

North, G. R., and R. F. Cahalan, 1981: Predictability in a solvable stochastic climate model. *J. Atmos. Sci.*, **38**, 504–513, doi:10.1175/1520-0469(1981)038<0504:PIASSC>2.0.CO;2.

——, J. Wang, and M. G. Genton, 2011: Correlation models for temperature fields. *J. Climate*, **24**, 5850–5862, doi:10.1175/2011JCLI4199.1.

Ragone, F., V. Lucarini, and F. Lunkeit, 2016: A new framework for climate sensitivity and prediction: A modelling perspective. *Climate Dyn.*, **46**, 1459–1471, doi:10.1007/s00382-015-2657-3.

Raper, S. C. B., J. M. Gregory, and T. J. Osborn, 2001: Use of an upwelling-diffusion energy balance climate model to simulate and diagnose A/OGCM results. *Climate Dyn.*, **17**, 601–613, doi:10.1007/PL00007931.

Rybski, D., A. Bunde, S. Havlin, and H. von Storch, 2006: Long-term persistence in climate and the detection problem. *Geophys. Res. Lett.*, **33**, L06718, doi:10.1029/2005GL025591.

——, ——, and H. von Storch, 2008: Long-term memory in 1000-year simulated temperature records. *J. Geophys. Res.*, **113**, D02106, doi:10.1029/2007JD008568.

Rypdal, K., 2012: Global temperature response to radiative forcing: Solar cycle versus volcanic eruptions. *J. Geophys. Res.*, **117**, D06115, doi:10.1029/2011JD017283.

——, 2016: Global warming projections derived from an observation-based minimal model. *Earth Syst. Dyn.*, **7**, 51–70, doi:10.5194/esd-7-51-2016.

——, L. Østvand, and M. Rypdal, 2013: Long-range memory in Earth's surface temperature on time scales from months to centuries. *J. Geophys. Res. Atmos.*, **118**, 7046–7062, doi:10.1002/jgrd.50399.

——, M. Rypdal, and H.-B. Fredriksen, 2015: Spatiotemporal long-range persistence in Earth's temperature field: Analysis of stochastic–diffusive energy balance models. *J. Climate*, **28**, 8379–8395, doi:10.1175/JCLI-D-15-0183.1.

Rypdal, M., 2016: Early-warning signals for the onsets of Greenland interstadials and the Younger Dryas–Preboreal transition. *J. Climate*, **29**, 4047–4056, doi:10.1175/JCLI-D-15-0828.1.

——, and K. Rypdal, 2014: Long-memory effects in linear response models of Earth's temperature and implications for future global warming. *J. Climate*, **27**, 5240–5258, doi:10.1175/JCLI-D-13-00296.1.

Sellers, W. D., 1969: A global climatic model based on the energy balance of the Earth–atmosphere system. *J. Appl. Meteor.*, **8**, 392–400, doi:10.1175/1520-0450(1969)008<0392:AGCMBO>2.0.CO;2.

Vyushin, D. I., P. J. Kushner, and F. Zwiers, 2012: Modeling and understanding persistence of climate variability. *J. Geophys. Res.*, **117**, D21106, doi:10.1029/2012JD018240.

Note about paper III

August 28, 2017
I found an error in the code for generating Figure 4 (a), resulting in shifting the black curve a factor 2π to the right. The result of this is the same as if we chose another set of time scales a factor 2π smaller than in the paper. Hence the time scales should be reduced if reproducing these figures, also when plotting the responses in Figure 3. As long as the residual spectrum is close to scale-invariant, the relative responses on each scale we determine from it remain approximately the same.